The Climatic Signature of Incised River Meanders

Colin P. Stark,[1]* Jonathan R. Barbour,[1] Yuichi S. Hayakawa,[2] Tsuyoshi Hattanji,[3] Niels Hovius,[4] Hongey Chen,[5] Ching-Weei Lin,[6] Ming-Jame Horng,[7] Kai-Qin Xu,[8,9] Yukitoshi Fukahata[10]

Climate controls landscape evolution, but quantitative signatures of climatic drivers have yet to be found in topography on a broad scale. Here we describe how a topographic signature of typhoon rainfall is recorded in the meandering of incising mountain rivers in the western North Pacific. Spatially averaged river sinuosity generated from digital elevation data peaks in the typhoon-dominated subtropics, where extreme rainfall and flood events are common, and decreases toward the equatorial tropics and mid-latitudes, where such extremes are rare. Once climatic trends are removed, the primary control on sinuosity is rock weakness. Our results indicate that the weakness of bedrock channel walls and their weakening by heavy rainfall together modulate rates of meander propagation and sinuosity development in incising rivers.

In humid, rapidly eroding (*1*) montane environments such as the Cascades (*2*), Japan (*3*), and Taiwan (*4*), lateral erosion along the banks and walls of bedrock-floored river channels (*5*–*13*) can be as important a process as vertical incision. Rates of lateral erosion can exceed down-cutting rates by over 10 times as a bedrock channel widens (*11*, *12*) or meanders (*5*–*10*, *13*, *14*). With time, such horizontal cutting is known to generate sinuous channels (*5*–*10*, *13*–*20*), very broad channels (*8*, *9*), bedrock-floored cut (strath) terraces (*2*, *5*, *6*, *13*, *21*), asymmetric valleys (*7*, *17*–*19*), and even meander cut-off loops (*8*–*10*, *13*, *15*–*20*). In particular, field observations (*8*–*10*) and theoretical considerations (*22*, *23*) indicate that the majority of the meanders and high sinuosities seen in such bedrock rivers are actively generated by erosive lateral chan-

nel motion (*5*–*9*), although there are certainly cases in which meandering forms are inherited (*15*) as channels maintain their sinuous shape during down-cutting (*19*, *20*).

Three key factors determine the rate of lateral channel erosion: (i) flood shear (*5*, *6*, *10*–*12*) and particle momentum flux (*24*) on the channel walls, which induce bedrock wear (*12*, *14*, *25*, *26*) and remove debris dumped from adjacent hill slopes; (ii) bedrock weakness (*5*, *6*, *9*, *25*, *26*), which sets both the basic rate of flow-driven wear (*25*) and the instability of channel bedrock walls and hill slopes (*27*); and (iii) rainfall intensity and duration, which modulate bedrock instability and adjust the rate of wall erosion by rock falls and landslides (*27*). Transient alluvial cover of the bedrock bed is also important, but only in the relative sense (*14*, *21*) of reducing down-cutting rates while leaving wall erosion rates unaffected.

These observations led us to pose two hypotheses: (i) The degree of sinuosity development in a network of bedrock rivers may provide a quantifiable measure of the rate of lateral channel erosion; and (ii) catchment-scale averaged sinuosity in humid mountain rivers should correlate on a regional scale both with rock type and with rainfall and flood frequency and magnitude. Underpinning these hypotheses is the observation (*19*) (fig. S2) that a range of phenomena—fluxes of debris from adjoining hill slopes, differential erosion into heterogeneous bedrock, big shifts in formative discharge through stream capture, catchment growth or shrinkage, and climate change, not to mention necking and loop cut-off—act to disrupt meander growth and ultimately limit the development of sinuosity. Over time, competition between lateral channel erosion and meander-limiting processes yields a spread of reach sinuosities across a catchment whose average is expected to depend on bedrock erodibility and climatic conditions.

Previous support for the two hypotheses comes from studies of laterally mobile bedrock rivers in Japan (*5*–*7*), where flood shear and rock strength were found to correlate well with horizontal erosion and lateral channel migration during 30,000 years of vertical incision. However, no studies of sinuosity have been attempted at a scale large enough to identify climatic trends, chiefly because the necessary data have not been available in consistent digital form at a regional scale. With the recent availability of 3-arc sec Shuttle Radar Topography Mission (SRTM) digital elevation model data for much of the globe, as well as digital geology maps and archives of meteorological and hydrologic data, this impediment no longer exists.

To test the two hypotheses, we quantified upland river sinuosity (Fig. 1, A and B) in the western North Pacific using SRTM data. We initially focused on Japan because of its broad dynamic range of storm rainfall. We processed a seamless, high-resolution, vector geology map of Japan (*3*) (Fig. 1, C and D) to identify incising bedrock channels, segment them into reaches between stream junctions, and group them into five broad lithological classes (*28*) that span areas sufficient for statistical analysis. Channel-reach sinuosities s for each of the five classes were then aggregated within 100-km moving windows and converted into gridded maps of regionalized average sinuosity χ (*28*).

Next, we correlated χ with daily rainfall statistics, generated from 20- to 30-year records from a dense network of 1666 stations (Fig. 2A) across the archipelago (*28*), to assess the dual influences of lithology and climate on sinuosity on a subregional scale. Scaling up to the western North Pacific, we generated a single grid of sinuosity χ for a group of lithologies chosen from the Japan analysis for their similar apparent erodibility (Fig. 2B). Finally, we correlated the sinuosity

[1]Lamont-Doherty Earth Observatory of Columbia University, Palisades, New York 10964, USA. [2]Center for Spatial Information Science, University of Tokyo, 5-1-5 Kashiwanoha, Kashiwa, Chiba 277-8568, Japan. [3]Graduate School of Life and Environmental Sciences, University of Tsukuba, Ibaraki 305-8572, Japan. [4]Department of Earth Sciences, University of Cambridge, Downing Street, Cambridge CB2 3EQ, UK. [5]Department of Geosciences, National Taiwan University, No. 1, Sec. 4, Roosevelt Road, Taipei 10617, Taiwan. [6]Department of Earth Sciences, National Cheng Kung University, Tainan, Taiwan. [7]Water Resources Agency, Ministry of Economic Affairs, Hsin-Yi Road, Taipei, Taiwan. [8]National Institute for Environmental Studies, 16-2 Onogawa, Tsukuba 305-8506, Japan. [9]State Key Laboratory of Water Resources and Hydropower Engineering Science, Wuhan University, Wuhan 430072, China. [10]Disaster Prevention Research Institute, Kyoto University, Gokasyo, Uji, Kyoto 611-0011, Japan.

*To whom correspondence should be addressed. E-mail: cstark@ldeo.columbia.edu

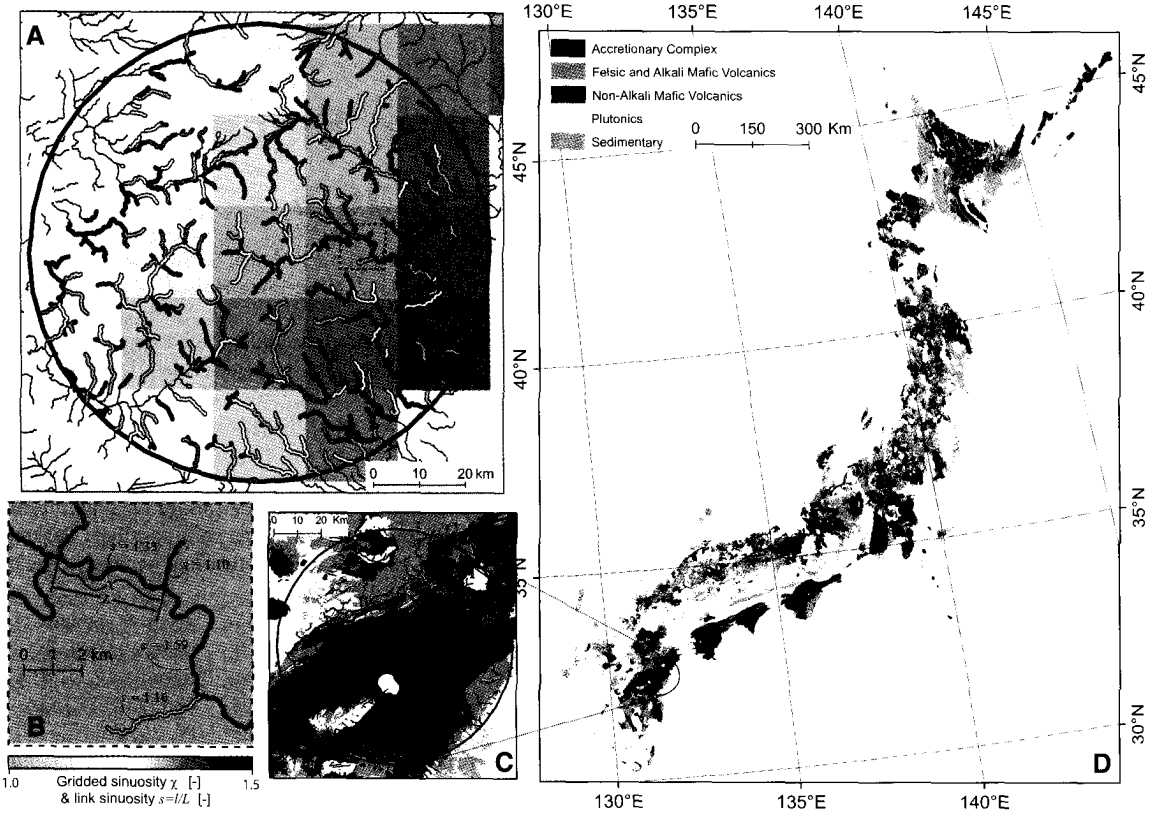

Fig. 1. **(A)** Drainage delineation and sinuosity calculation. **(B)** A zoom shows how each reach sinuosity $s = l/L$ is the ratio of along-stream l to the distance the crow flies L between channel junctions. Regionalized sinuosity χ is the weighted sum (*28*) of the link sinuosities within the 100-km-diameter circle in **(A)** and **(C)**; χ is gridded at a resolution of 20 km. **(D)** Simplified bedrock geology of Japan based on a 1:200,000 synthesis carried out by the Geological Survey of Japan. Large contiguous areas of Quaternary sediments are indicated in gray, as are metamorphic rocks, which represent a very small fraction of total bedrock exposure; both are excluded from sinuosity analysis. Regionalized sinuosity χ was mapped by delineating reach sinuosities on each lithology mask separately.

grid with typhoon-track (Fig. 3), stream-gauge, and rain-gauge data (Fig. 4) around the western Pacific Rim (*28*).

In the Japan analysis, spatial correlation of the sinuosity χ grid with station rainfall statistics [such as frequency of rainfall exceedance F_{rx} of 50 mm/day (*28*)] revealed approximately linear trends (table S1) for almost all rock types (Fig. 2A), with sinuosity χ rising with increasing "storminess" from north to south. To isolate the dependence on rock type (Fig. 2), values of χ were projected from a common origin onto a reference F_{rx} =10 year^{-1}, and a probability density function (PDF) $p(\chi)$ was generated for each lithology class.

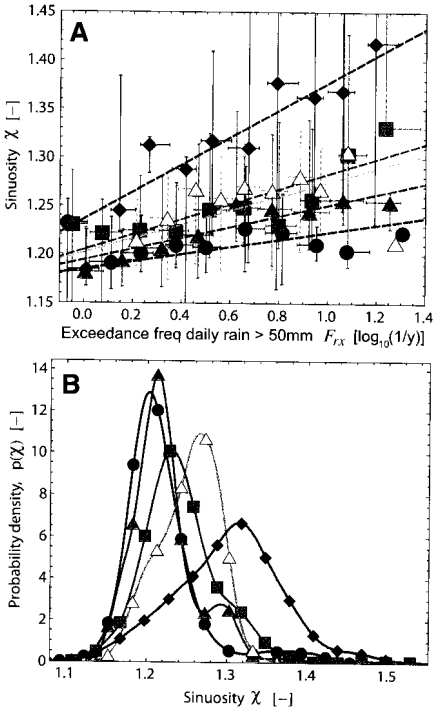

Fig. 2. **(A)** Sinuosity χ versus storminess expressed as the frequency F_{rx} at which rainfall accumulation exceeds 50 mm in 24 hours; **(B)** PDFs of detrended sinuosity $p(\chi|F_{rx} = 10)$, generated by projecting each value of $\chi(F_{rx})$ onto $\chi(10)$ along lines with a common origin at $\chi = 1.16$ (the estimated average for all the data combined). Blue diamonds, accretionary complex; green squares, nonaccretionary complex sedimentary rock; yellow triangles, plutonics; orange triangles, felsic and alkali mafic volcanics; purple circles, nonalkali mafic volcanics; dashed lines, linear regressions. Error bars are 1σ SDs.

The PDFs show (Fig. 2B) that the most sinuous incising rivers are found in accretionary complex lithologies (*8*, *9*). These rocks are predominantly low-strength, highly erodible (*6*, *8*, *9*), silt and fine-sand turbidites with intermittent coarser, stronger units; channels cut into these rocks are known for their high degree of meandering (*8*, *9*). The least sinuous incising rivers are found in generally erosion-resistant (*5*), nonalkali mafic volcanics, which include rocks ranging in strength from very strong, fresh basaltic lavas to weathered, unwelded, much weaker tuffs (*5*). The greatest regional variation in sinuosity χ and its strongest correlation with F_{rx} are seen in the weak accretionary complex rocks, whereas the strong, nonalkali mafic volcanics show the least variation in χ and its weakest correlation with F_{rx} (Fig. 2A and table S1).

When combined with past studies of erosion rates and fractured rock strength in Japan (*5*, *6*), our results (Fig. 2 and table S1) indicate that rock erodibility (*5*, *6*, *9*, *25*) is the primary control on sinuosity development and incised meandering (*8*, *9*). Heavy rainfall frequency or storminess exerts a clear secondary control on sinuosity development, particularly in weaker rock types.

Next we examined sinuosity correlations on a subhemispheric scale. By combining the high-resolution geology data in Japan with low-resolution digital geology for the western North

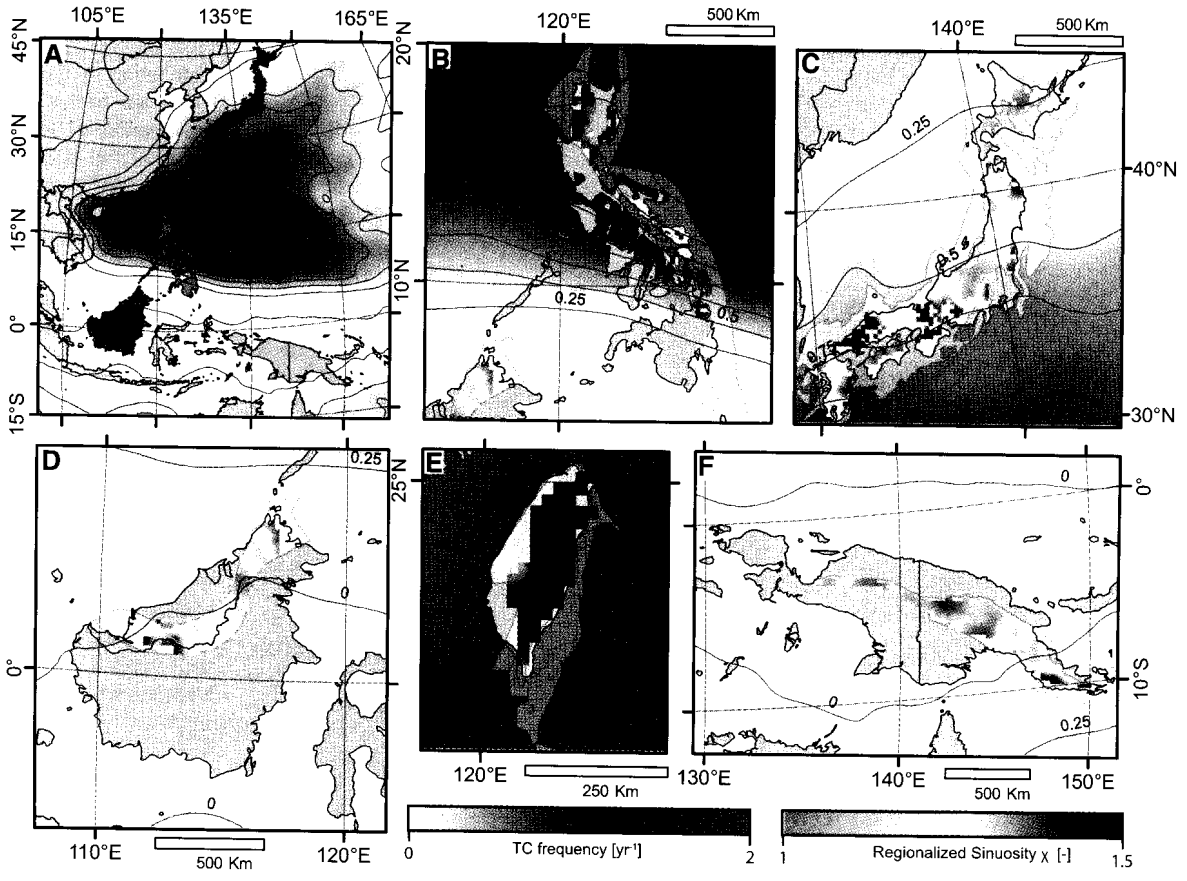

Fig. 3. **(A)** Regionalized sinuosity χ (green/yellow/red for range 1 to 1.5) and typhoon strike frequency (blue contour intervals of 0.25 per year) across the western North Pacific. The studied islands are shown as follows: **(B)** the Philippines (green), **(C)** Japan (dark blue), **(D)** Borneo (brown), **(E)** Taiwan (purple), and **(F)** New Guinea (cyan). Analysis was restricted to high-relief areas on subduction complex lithologies chosen from the Japan analysis for similarity in their apparent erodibility; masked-out regions are shown in gray.

Pacific, we were able to restrict χ mapping to a subset of lithologies (mafic and nonmafic volcanics, plutonics, and sedimentary rocks) with broadly similar sensitivity of sinuosity to storm frequency F_{TX} (Fig. 2). We excluded geological formations dissimilar to those found in Japan (such as those in southern Borneo), whose sinuosity sensitivity was not calibrated by the Japan analysis. The resulting clipping mask for this geological assemblage was used to prune the stream networks and generate another map of sinuosity χ spanning an area from the equatorial tropics to the mid-latitudes (Fig. 3).

We correlated (Fig. 4) the regional sinuosity χ grid with records of monthly mean rainfall, daily river discharge data, and a spatial PDF of typhoon strike frequency (Fig. 3) generated from tropical cyclone track records (*28*). We found roughly linear trends in sinuosity with both rainfall variability, expressed as the coefficient of variation R_{cv} [Fig. 4A; Kendall's rank correlation coefficient (τ_k) = 0.44, Pearson's correlation coefficient (r^2) = 0.40], and with relative flood intensity, expressed as the 99th percentile discharge normalized by catchment area Q_{99}/A (Fig. 4B; $\tau_k = 0.48$, $r^2 = 0.42$). Sinuosity is highest in the monsoonal, typhoon-prone northern Philippines, southern Japan, and Taiwan, where heavy rainfall frequency and flood intensity are highest (*1*, *3*, *4*, *29*). Low-sinuosity rivers are more commonly found in mid-latitude northern Japan and in the equatorial tropics, where extremely heavy storms are far less frequent and flood variability is much lower. This regional dependence on storm climatology is confirmed by the correlation seen between sinuosity and typhoon strike frequency (Fig. 4C; $\tau_k = 0.50$, $r^2 = 0.45$) and is corroborated by the peaked relationship seen between sinuosity and latitude (Fig. 4D).

Our combined results show that once account is taken of rock type, sinuosity records a measurable signature of storminess—a key factor in climate-landscape dynamics (*30*). Conversely, our observations show that if the modulating effect of storminess is removed, sinuosity provides a proxy measure for bedrock erodibility.

This dependence of sinuosity χ on bedrock erodibility (Fig. 2), as well as the ubiquitous association of incised meanders with weak bedrock (*5*, *6*, *8*–*10*, *13*, *20*), indicates that horizontal channel erosion rates are much more sensitive to greater rock erodibility than are vertical channel erosion rates. This asymmetry lies in the dual control of lateral channel motion by both flow-driven wear of the channel wall (*12*, *24*, *26*) and mass-wasting erosion of the adjoining hill slope, versus the single control on vertical incision by flow-driven wear of the bed alone (*14*, *25*). Bed sediment cover augments the asymmetry (*14*) but is not its cause.

The climatic signature expressed in sinuosity comes from an amplification of this asymmetric sensitivity. More frequent heavy rainfall means that channel walls and adjoining hill slopes are destabilized more often and are more prone to lateral erosion (*27*); it also means an increase in flood frequency, flow shear, and sediment momentum flux on both channel walls and beds. The combined effect is to raise wall erosion rates more than bed erosion rates and to accelerate sinuosity development (fig. S2). In the western North Pacific, this phenomenon ultimately leads to a correlation between typhoon strike frequency and incised channel sinuosity.

The strength of the observed climatic signature underlines the strong coupling between climate and erosion in these island mountain landscapes (*1*, *4*, *29*, *30*) and the extent to which their morphology reflects recent [late Pleistocene to present (*5*, *6*, *13*)] climatic conditions. This coupling is much weaker where erosion rates are much lower, and therefore sinuosity development in such environments [such as the Colorado Plateau (*20*)] will reflect a much longer-term integration of weather patterns.

Even for the western North Pacific there is significant disparity between the brief time span of available meteorological and hydrologic data [~20 to 60 years (*28*)] versus the time scale over which bedrock meanders have evolved [~1000 to ~100,000 years (*5*, *6*, *13*)]. We nevertheless have confidence that our correlations with storminess have meaning, because the regional pattern of storminess is so strongly tied to the average distribution of typhoon tracks (Figs. 3 and 4). The shape of this distribution is determined by the location of tropical cyclogenesis (currently between 8°N and 25°N in the western North Pacific) and by the steering effect of the large-scale circulation of the atmosphere (*31*). Both undoubtedly change on interannual to multimillenial time scales, but it is reasonable to infer that the broad latitudinal trend in typhoon strikes, with its peak in the subtropics (Fig. 4D), has remained roughly constant since the current plate-tectonic configuration of the western North Pacific was established several million years ago.

The studied landscapes and their high sediment fluxes also exhibit a strong coupling with tectonics (*1*, *4*, *30*), but our results suggest that rock uplift rate is a much less plausible explanatory variable for sinuosity χ than climate. Sinuosities are highest in the northern Philippines (Luzon; Figs. 3 and 4) and second highest in Taiwan, which is consistent with our observation that typhoon strike frequencies and storminess measures are highest in Luzon and second highest in Taiwan, but is inconsistent with the relatively low late Pleistocene–Holocene uplift rates seen in Luzon (~1 mm/year) (*32*) as compared with those in Taiwan [~6 mm/year (*4*, *30*, *33*)]. Similarly, the north-south trend in increasing sinuosity seen in Japan (Fig. 2A) is not expressed in the regional

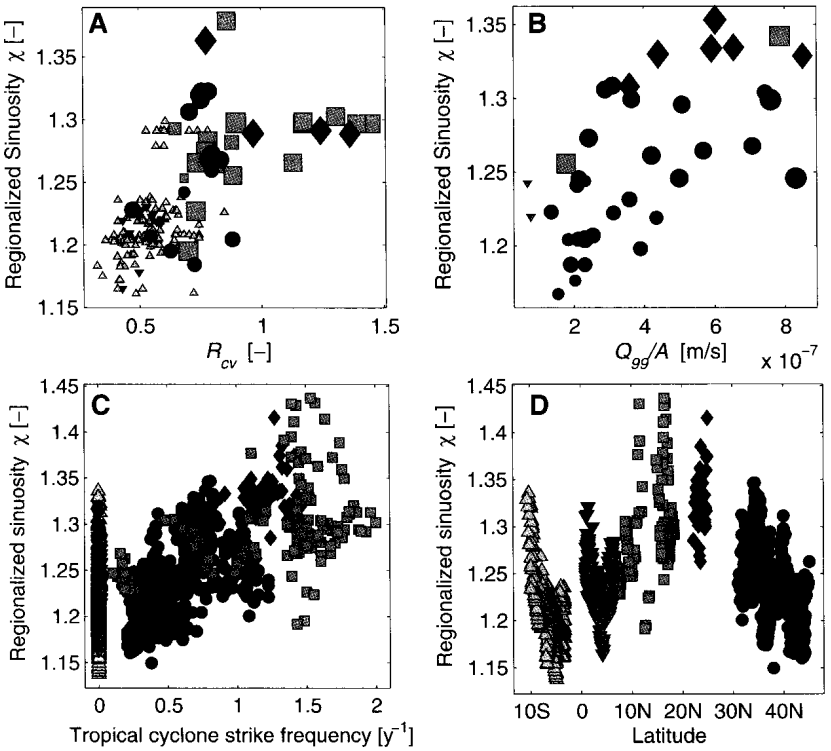

Fig. 4. Regional correlation analyses of sinuosity χ. Colors and symbols are as follows: dark blue circles, Japan; purple diamonds, Taiwan; green squares, the Philippines; brown downward triangles, Borneo; cyan upward triangles, New Guinea. **(A)** With coefficient of variation $R_{cv} = R_\sigma/R_\mu$ (where σ is standard deviation and μ is the mean) of monthly rainfall at 169 rain gauges across the western North Pacific ($\tau_k = 0.44$, $r^2 = 0.40$). Symbol sizes correspond to typhoon strike frequency. **(B)** With relative flood intensity Q_{99}/A (99th percentile discharge normalized by catchment area A) measured at 38 river gauges across the western North Pacific ($\tau_k = 0.48$, $r^2 = 0.42$). **(C)** With typhoon strike frequency ($\tau_k = 0.50$, $r^2 = 0.45$; excluding Borneo and New Guinea where typhoons are absent). **(D)** With latitude, showing a peak in the typhoon-dominated subtropics.

pattern of uplift rates inferred from marine isotope stage 5.5 marine terrace elevations (*33*). If uplift rate does play a role, it may be in modulating channel steepness as a function of sinuosity (fig. S3).

References and Notes

1. J. D. Milliman, J. P. M. Syvitski, *J. Geol.* **100**, 525 (1992).
2. F. J. Pazzaglia, M. T. Brandon, *Am. J. Sci.* **301**, 385 (2001).
3. Y. S. Hayakawa, T. Oguchi, *Geomorphology* **111**, 27 (2009).
4. S. J. Dadson *et al.*, *Nature* **426**, 648 (2003).
5. T. Suzuki, *Trans. Jpn. Geomorphol. Union* **3-1**, 1 (1982).
6. T. Suzuki, *Trans. Jpn. Geomorphol. Union* **4-1**, 33 (1983).
7. M. Hirano, *Trans. Jpn. Geomorphol. Union* **1-2**, 117 (1981).
8. R. Yagi, H. Ikeda, *Bull. Environ. Res. Center Univ. Tsukuba* **22**, 1 (1997).
9. A. Nakano, H. Ikeda, *Bull. Environ. Res. Center Univ. Tsukuba* **24**, 1 (1999).
10. J. R. Barbour *et al.*, *Geophys. Res. Lett.* **36**, L04401 (2009).
11. C. P. Stark, *Geophys. Res. Lett.* **33**, L04402 (2006).
12. J. M. Turowski, D. Lague, N. Hovius, *J. Geophys. Res.* **114** (F3), F03016 (2009).
13. J. B. H. Shyu, K. Sieh, J.-P. Avouac, W.-S. Chen, Y.-G. Chen, *J. Geophys. Res.* **111** (B8), B08403 (2006).
14. J. M. Turowski, D. Lague, N. Hovius, *J. Geophys. Res.* **112**, (F4), F04006 (2007).
15. W. M. Davis, *Science* **21**, 225 (1893).
16. A. Winslow, *Science* **22**, 31 (1893).
17. R. H. Mahard, *J. Geomorphol.* **5**, 32 (1942).
18. H. Blank, *Geol. Soc. Am. Bull.* **81**, 3135 (1970).
19. G. H. Dury, *Am. J. Sci.* **252**, 193 (1954).
20. D. R. Harden, *Geol. Soc. Am. Bull.* **102**, 233 (1990).
21. G. S. Hancock, R. S. Anderson, *Geol. Soc. Am. Bull.* **114**, 1131 (2002).
22. S. Ikeda, G. Parker, K. Sawai, *J. Fluid Mech.* **112**, 363 (1981).
23. G. Seminara, *J. Fluid Mech.* **554**, 271 (2006).
24. J. G. A. Bitter, *Wear* **6**, 169 (1963).
25. L. S. Sklar, W. E. Dietrich, *Geology* **29**, 1087 (2001).
26. K. Hartshorn, N. Hovius, W. B. Dade, R. L. Slingerland, *Science* **297**, 2036 (2002).
27. F. Guzzetti, S. Peruccacci, M. Rossi, C. P. Stark, *Meteorol. Atmos. Phys.* **98**, 239 (2007).
28. See supporting material on *Science* Online.
29. J. Galewsky *et al.*, *J. Geophys. Res.* **111** (F3), F03014 (2006).
30. S. D. Willett *et al.*, Eds., *GSA Spec. Pap. 398, Penrose Conf. Ser.* (2006).
31. J. C. L. Chan, *Annu. Rev. Fluid Mech.* **37**, 99 (2005).
32. Y. Maeda *et al.*, *Quat. Int.* **115–116**, 15 (2004).
33. Y. Ota, M. Yamaguchi, *Quat. Int.* **120**, 105 (2004).

34. This study was supported by NASA , NSF (Earth Sciences Division, Geomorphology and Land-use Dynamics Program), and the Taiwan National Science Council. We thank W. E. Dietrich, G. Parker, and E. E. Wohl for enlightening discussions and C.-H. Jen, C. Huang, T.-C. Yi, and M. Tajikara for help in the field.

Supporting Online Material

www.sciencemag.org/cgi/content/full/327/5972/1497/DC1
Methods
Figs. S1 to S3
Table S1

9 November 2009; accepted 5 February 2010
10.1126/science.1184406